Fluoroaromatic–Fluoroaromatic Interactions between Inhibitors Bound in the Crystal Lattice of Human Carbonic Anhydrase II

Chu-Young Kim,[†] Pooja P. Chandra,[‡] Ahamindra Jain,[§] and David W. Christianson*,[†]

Contribution from the Roy and Diana Vagelos Laboratories, Department of Chemistry, University of Pennsylvania, Philadelphia, Pennsylvania 19104-6323, Department of Chemistry, Swarthmore College, Swarthmore, Pennsylvania 19081-1397, and the Department of Chemistry, University of California, Berkeley, California 94720-1460

Abstract: Intermolecular interactions of eleven different fluoroaromatic inhibitors are probed within the scaffolding of the crystal lattice of Phe-131→Val carbonic anhydrase II. The degree and pattern of fluorine substitution on the inhibitor benzyl ring modulate its size, shape, and electronic character. In turn, these properties affect the geometry of intermolecular interactions between the fluoroaromatic rings of two different inhibitor molecules bound in the crystal lattice, as determined by X-ray crystallography. Depending on the degree and pattern of fluorine substitution, we observe a face-to-face (aromatic–aromatic) interaction, an atom-to-face (carbonyl–aromatic) interaction, or no interaction at all. These interaction geometries are analyzed with regard to van der Waals, electrostatic, and possible charge-transfer effects. For the aromatic–aromatic interactions investigated in this study, with aromatic ring quadrupoles specifically "tuned" by the degree and pattern of fluorination, the structural results suggest that London forces and charge-transfer complexation dominate over weakly polar electrostatic interactions in the association of aromatic ring pairs.

Introduction

The fundamental basis of attractive interactions between aromatic moieties is not thoroughly understood, partly because of apparent differences in the preferred geometries of such interactions. In DNA, bases are stacked in a face-to-face manner, which facilitates interstrand hydrogen bonding and stabilizes the double helix.[1] In contrast, aromatic side chains in refined protein structures tend to prefer an edge-to-face geometry, which contributes to tertiary structure stabilization.[2] Because nucleic acid bases are heteroaromatic with varied structures and electronic properties, it is likely that the electronic properties of the aromatic ring as well as its structural context play a significant role in directing the preferred geometries of intermolecular interactions.

Theoretical calculations show that the benzene homodimer preferentially forms an edge-to-face complex because of the large quadrupole moment associated with benzene;[2–5] a face-to-face arrangement would result in electrostatic repulsion (Figure 1). Consistent with preferred edge-to-face aromatic–aromatic interactions, benzene molecules pack in the crystal lattice with an edge-to-face, herringbone-like pattern.[6] Recently,
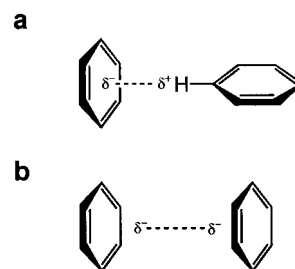

Figure 1. (a) Edge-to-face benzene dimer (attractive electrostatic interaction); (b) face-to-face benzene dimer (repulsive electrostatic interaction).

Wilcox and colleagues[7] and Cammers-Goodwin and colleagues[8] have reported elaborate small molecules in which two substituted benzene rings are brought into close contact by a semirigid linker. Surprisingly, these experiments indicate that the intramolecular aromatic–aromatic interactions appear to be dominated not by the interactions between aromatic ring quadrupoles but instead by dispersion forces.

Here, we report a novel system for the study of weak aromatic interactions: crystalline Phe-131→Val carbonic anhydrase II (F131V CAII) complexed with various fluoroaromatic inhibitors. CAII is a prototypical zinc enzyme, and it catalyzes the hydration of carbon dioxide to yield bicarbonate ion and a proton.[9–12] The inhibitors used in this study are fluorinated

* Address correspondence to Prof. David W. Christianson. Phone: (215) 898-5714. Fax: (215) 573–2201. E-mail: chris@xtal.chem.upenn.edu.
† University of Pennsylvania.
‡ Swarthmore College.
§ University of California, Berkeley.

(1) Saenger, W. *Principles of Nucleic Acid Structure*; Springer-Verlag: New York, 1984.
(2) Burley, S. K.; Petsko, G. A. *Adv. Protein Chem.* **1988**, *39*, 125–192.
(3) Jorgensen, W. L.; Severance, D. L. *J. Am. Chem. Soc.* **1990**, *112*, 4768–4774.
(4) Hunter, C. A.; Sanders, J. K. M. *J. Am. Chem. Soc.* **1990**, *112*, 5525–5534.
(5) Niesse, J. A.; Mayne, H. R. *J. Comput. Chem.* **1997**, *18*, 1233–1244.

(6) Cox, E. G.; Cruickshank, D. W. J.; Smith, J. A. S. *Proc. R. Soc. London* **1958**, *247*, 1–21.
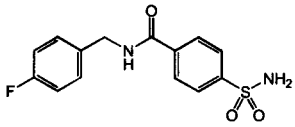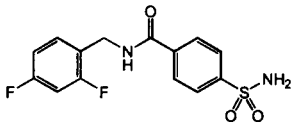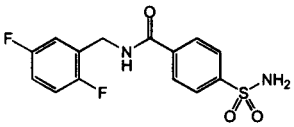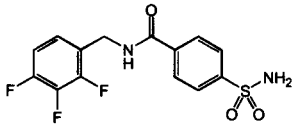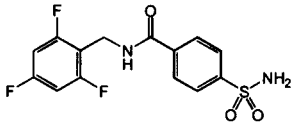(7) Kim, E.-I.; Paliwal, S.; Wilcox, C. S. *J. Am. Chem. Soc.* **1998**, *120*, 11192–11193.
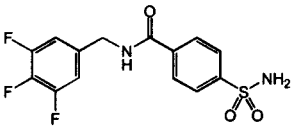(8) Martin, C. B.; Mulla, H. R.; Willis, P. G.; Cammers-Goodwin, A. *J. Org. Chem.* **1999**, *64*, 7802–7806.
(9) Coleman, J. E. *J. Biol. Chem.* **1967**, *242*, 5212–5219.
(10) Silverman, D. N.; Lindskog, S. *Acc. Chem. Res.* **1988**, *21*, 30–36.
(11) Sly, W. S.; Hu, P. Y. *Annu. Rev. Biochem.* **1995**, *64*, 375–401.

Table 1. Fluorinated F131V CAII Inhibitors[a]

4-fluoro-SBB (K_d = 3.3 nM)	2,4-difluoro-SBB (K_d = 3.3 nM)	2,5-difluoro-SBB (K_d = 2.2 nM)
4-(aminosulfonyl)-N-[(4-fluorophenyl)methyl]-benzamide	4-(aminosulfonyl)-N-[(2,4-difluorophenyl)methyl]-benzamide	4-(aminosulfonyl)-N-[(2,5-difluorophenyl)methyl]-benzamide
2,3,4-trifluoro-SBB (K_d = 3.8 nM)	2,4,6-trifluoro-SBB (K_d = 3.9 nM)	3,4,5-trifluoro-SBB (K_d = 3.9 nM)
4-(aminosulfonyl)-N-[(2,3,4-trifluorophenyl)methyl]-benzamide	4-(aminosulfonyl)-N-[(2,4,6-trifluorophenyl)methyl]-benzamide	4-(aminosulfonyl)-N-[(3,4,5-trifluorophenyl)methyl]-benzamide

[a] K_d values reflect inhibitor dissociation from the primary binding site.[14]
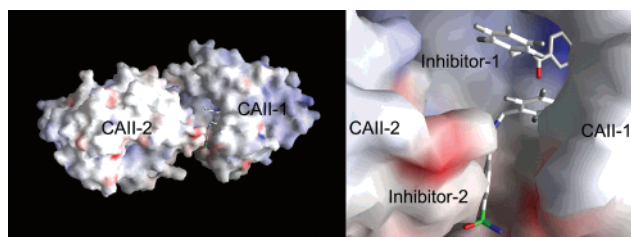

Figure 2. F131V CAII−2,3,4,5,6-pentafluoro-SBB complex. Inhibitor-1 binds in the active site of CAII-1. Inhibitor-2 binds in a cleft formed by the CAII-1/CAII-2 interface in the crystal lattice. CAII-2 is located at position −x, y + ¹/₂, −z, relative to CAII-1.

derivatives of 4-(aminosulfonyl)-*N*-phenylmethylbenzamide (SBB), a competitive inhibitor of native and F131V CAIIs (Table 1).[13] Notably, each inhibitor bears a different degree and pattern of fluorination.

Crystalline F131V CAII contains two binding sites that accommodate fluorobenzyl phenylsulfonamides (Figure 2). The primary binding site is located in the active site of the enzyme. This is the binding site typically occupied by sulfonamide inhibitors, each of which coordinates to the active site zinc ion through an ionized sulfonamide nitrogen.[16−19] The secondary binding site is a hydrophobic cleft formed between CAII molecules at positions x, y, z and −x, y + ¹/₂, −z in the crystal lattice. This site was first observed occupied by the second

molecule of phenol in the CAII−phenol₂ complex.[20] Because of the proximity of the binding sites and the geometry of inhibitor binding, fluorobenzyl phenylsulfonamides that occupy both sites can interact with each other through their fluoroaromatic rings. Systematic substitution of fluorine atoms for benzyl hydrogen atoms modulates the electronic character of the interacting aromatic rings, thereby perturbing the balance of various intermolecular forces between the two rings. We study the structural consequences of varying inhibitor fluorination using X-ray crystallography. Analysis of the binding conformations of the inhibitors shown in Table 1 and comparison with previously reported enzyme−fluoroaromatic inhibitor complexes[15] yield five examples of fluoroaromatic inhibitor binding to both primary and secondary sites. The structural basis for this novel binding behavior is attributable to the pattern of fluorine substitution.

There are two key advantages to this enzyme-based study of intermolecular fluoroaromatic interactions. First, the two fluoroaromatic groups are bound and isolated within the protein scaffolding, not readily influenced by other effects. For example, the inhibitor molecules themselves do not direct crystal lattice formation or stabilization, so we avoid the influence of multiple aromatic interactions or crystal lattice artifacts that potentially accompany small molecule crystallographic studies. Additionally, our system comprises a true bimolecular aromatic dimer, which complements the covalently linked, unimolecular aromatic pairs used in other studies.[7,8]

Results

The electron density maps in Figure 3 correspond to enzyme complexes with the six fluoroaromatic inhibitors shown in Table 1. In Figure 4, the structures of these complexes are compared with those of 5 previously described enzyme−fluoroaromatic inhibitor complexes.[15] The binding conformation of each inhibitor in the primary binding site (i.e., the active site of F131V CAII) is quite similar: the ionized sulfonamide nitrogen coordinates to zinc and displaces the zinc-bound hydroxide ion of the native enzyme; this nitrogen also donates a hydrogen bond to the hydroxyl group of Thr-199. One sulfonamide oxygen

(12) Christianson, D. W.; Fierke, C. A. *Acc. Chem. Res.* **1996**, *29*, 331−339.

(13) Cappalonga Bunn, A. M.; Alexander, R. S.; Christianson, D. W. *J. Am. Chem. Soc.* **1994**, *116*, 5063−5068.

(14) Doyon, J. B.; Hansen, E. A. M.; Kim, C.-Y., Chang, J. S.; Christianson, D. W.; Madder, R. D.; Voet, J. G.; Baird, T. A., Jr.; Fierke, C. A.; Jain, A. *Org. Lett.* **2000**, *2*, 1189−1192.

(15) Kim, C.-Y.; Chang, J. S.; Doyon, J. B.; Baird, T. T., Jr.; Fierke, C. A.; Jain, A.; Christianson, D. W. *J. Am. Chem. Soc.* **2000**, *122*, 12125−12134.

(16) Boriack-Sjodin, P. A.; Zeitlin, S.; Chen, H.-H.; Crenshaw, L.; Gross, S.; Dantanarayana, A.; Delgado, P.; May, J. A.; Dean, T.; Christianson, D. W. *Protein Sci.* **1998**, *7*, 2483−2489.

(17) Håkansson, K.; Liljas, A. *FEBS Lett.* **1994**, *350*, 319−322.

(18) Baldwin, J. J.; Ponticello, G. S.; Anderson, P. S.; Christy, M. E.; Murcko, M. A.; Randall, W. C.; Schwam, H.; Sugrue, M. F.; Springer, J. P.; Gautheron, J.; Grove, J.; Mallorga, P.; Viader, M.; McKeever, B. M.; Navia, M. A. *J. Med. Chem.* **1989**, *32*, 2510−2513.

(19) Håkansson, K.; Carlsson, M.; Svensson, L. A.; Liljas, A. *J. Mol. Biol.* **1992**, *227*, 1192−1204.

(20) Nair, S. K.; Ludwig, P. A.; Christianson, D. W. *J. Am. Chem. Soc.* **1994**, *116*, 3659−3660.
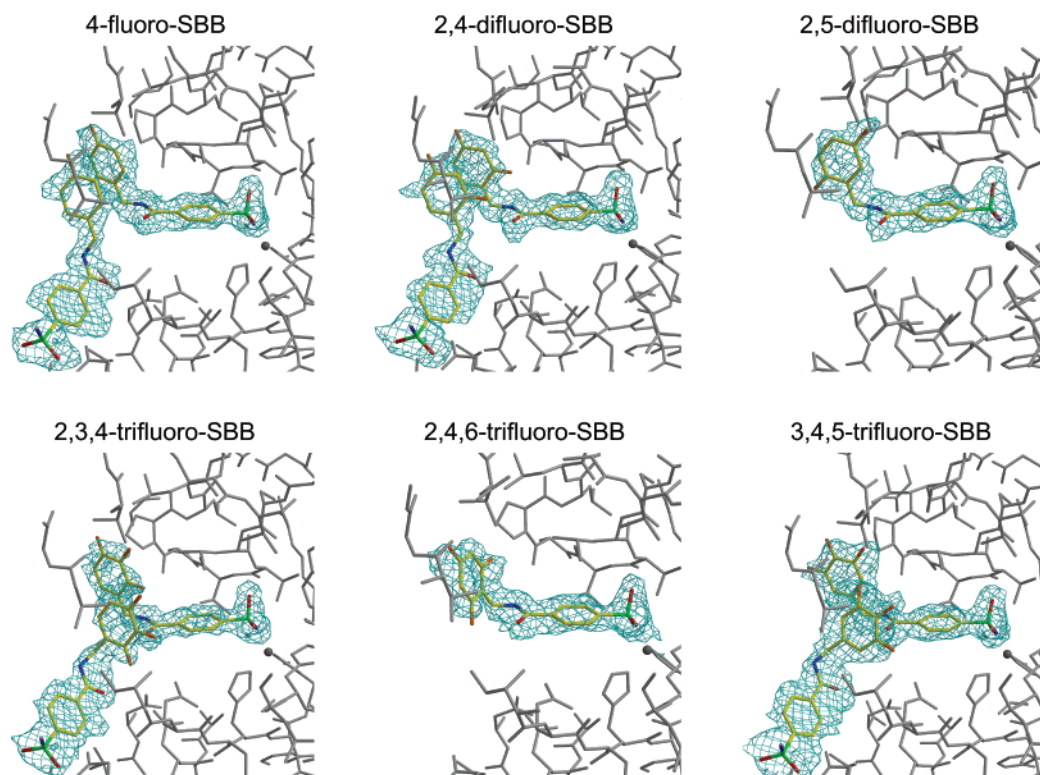
Figure 3. X-ray crystal structures of F131V CAII−inhibitor complexes with 4-fluoro-SBB, 2,4-difluoro-SBB, 2,5-difluoro-SBB, 2,3,4-trifluoro-SBB, 2,4,6-trifluoro-SBB, and 3,4,5-trifluoro-SBB. Difference electron density maps calculated with Fourier coefficients $|F_o| - |F_c|$ and phases derived from the final model less the inhibitor and active site solvent molecules. Maps are contoured at 2.2σ.

accepts a hydrogen bond from the backbone NH group of Thr-199, and the other sulfonamide oxygen makes no interactions.

In the F131V CAII complexes with perhydro-SBB, 2-fluoro-SBB, 2,3-difluoro-SBB, 2,5-difluoro-SBB, 2,6-difluoro-SBB, and 2,4,6-trifluoro-SBB, the secondary binding site is unoccupied. In the F131V CAII complexes with 4-fluoro-SBB and 2,4-difluoro-SBB, the fluoroaromatic ring of the first inhibitor (in the primary binding site) makes a nearly perfect face-to-face contact with the fluoroaromatic ring of the second inhibitor (in the secondary binding site) (Figure 5a). In the F131V CAII complexes with 2,3,4-trifluoro-SBB, 3,4,5-trifluoro-SBB, and 2,3,4,5,6-pentafluoro-SBB, the fluoroaromatic ring of the second inhibitor makes an atom-to-face contact with the carbonyl oxygen of the first inhibitor (Figure 5b). The geometries of fluoroaromatic−fluoroaromatic and fluoroaromatic−carbonyl interactions are summarized in Table 2. In all instances where the secondary binding pocket is occupied, the un-ionized sulfonamide nitrogen of the second inhibitor donates a hydrogen bond to Asp-72; no other enzyme−inhibitor hydrogen bonds are observed. The binding of 2,3,4,5,6-pentafluoro-SBB illustrated in Figure 2 reveals a significant intermolecular cleft that accommodates the binding of the second inhibitor molecule. This cleft is widest in the vicinity of the fluoroaromatic rings, so the protein environment does not appear to substantially impact the interaction geometry of the fluoroaromatic rings.

Discussion

Intermolecular Interactions between Aromatic Rings. The analysis of aromatic−aromatic interactions between fluoroaromatic inhibitors that occupy both primary and secondary binding sites can be simplified by considering four principal energetic contributions. First, induced-dipole−induced-dipole interactions (Figure 6a) occur when molecules are in contact: also known

as London forces or dispersion forces, these van der Waals interactions are always attractive. Second, dipole−dipole electrostatic interactions (Figure 6b) are possible because of the highly electronegative fluorine atoms: all fluorinated aromatic rings have a permanent dipole moment. Depending on the relative orientation of the fluoroaromatic rings, dipole−dipole interactions can be attractive or repulsive. Third, quadrupole−quadrupole electrostatic interactions (Figure 6c) can occur because of the substantial quadrupole moments of aromatic systems (Table 3); these electronic moments are a consequence of delocalized π electrons. For identical aromatic ring pairs oriented with face-to-face geometry, these interactions will be repulsive. Finally, aromatic ring pairs can form attractive $\pi \rightarrow \pi^*$ charge-transfer complexes (Figure 6d). Charge-transfer complexation requires close proximity and face-to-face geometry, features which can readily be determined by X-ray crystallographic analysis.

Which of these four energetic contributions dominates the interactions of fluoroaromatic inhibitor pairs interacting in the crystal lattice of F131V CAII? Face-to-face aromatic−aromatic interactions are observed in the complexes with 4-fluoro-SBB and 2,4-difluoro-SBB (Figure 5a). The van der Waals interactions between fluoroaromatic rings make an attractive contribution. However, repulsive contributions from dipole−dipole and quadrupole−quadrupole interactions arise from the parallel orientation of fluoroaromatic ring dipoles with face-to-face geometry. However, because the face-to-face geometry of the fluoroaromatic ring pairs would facilitate the formation of a charge-transfer complex, we advance that such complexation may additionally stabilize the face-to-face interactions of the fluoroaromatic rings. Because alternative fluoroaromatic ring conformations (e.g., with edge-to-face geometry) could be accommodated within the wide intermolecular cleft visible in Figure 2, we conclude that van der Waals interactions and
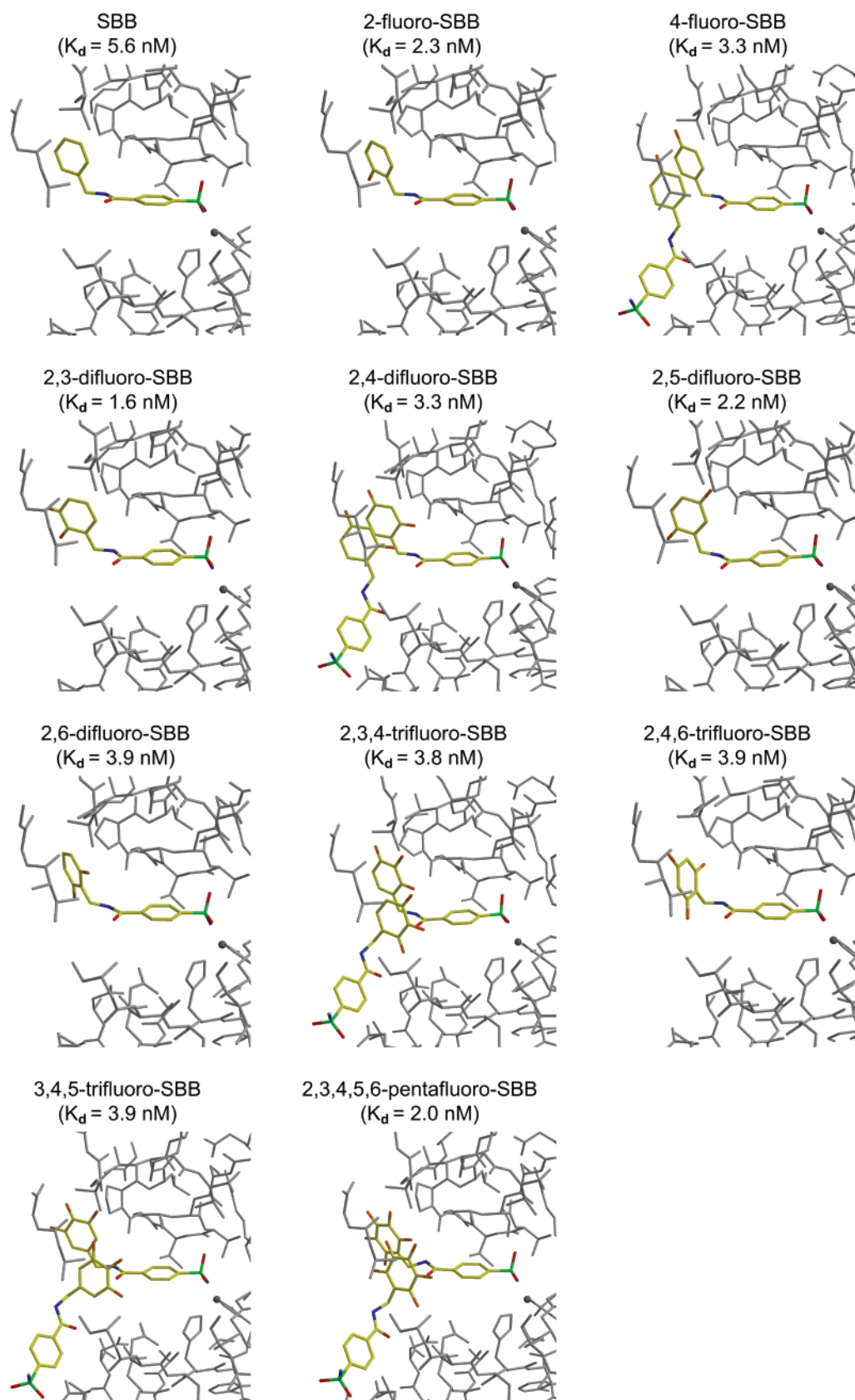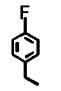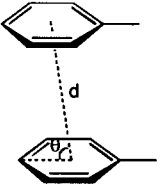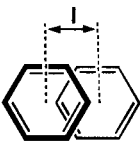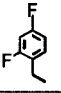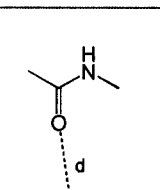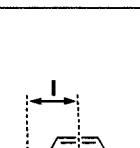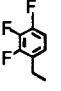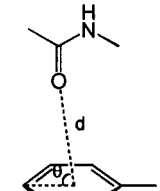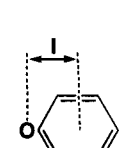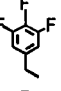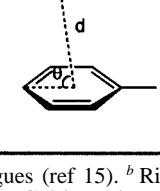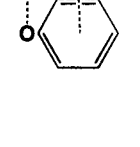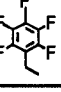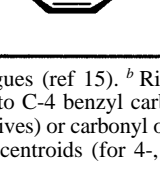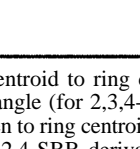
Figure 4. X-ray crystal structures of F131V CAII−inhibitor complexes with SBB, 2-fluoro-SBB, 4-fluoro-SBB, 2,3-difluoro-SBB, 2,4-difluoro-SBB, 2,5-difluoro-SBB, 2,6-difluoro-SBB, 2,3,4-trifluoro-SBB, 2,4,6-trifluoro-SBB, 3,4,5-trifluoro-SBB, and 2,3,4,5,6-pentafluoro-SBB. Inhibitor K_d values[14] are indicated in parentheses.

potential charge-transfer complexation dominate over weakly polar interactions (e.g., dipole−dipole, quadrupole−quadrupole) in the binding of these fluoroaromatic inhibitor pairs.

Fluoroaromatic−carbonyl interactions are observed for inhibitor pairs with 2,3,4-trifluoro-SBB, 3,4,5-trifluoro-SBB, and 2,3,4,5,6-pentafluoro-SBB because of a conformational change

Table 2.   Inhibitor−Inhibitor Interaction Geometry

Fluorination pattern		Interaction geometry		θ^b	d^c	l^d
	4			72.1°	4.4 Å	1.4 Å
	2,4			81.1°	3.8 Å	0.6 Å
	2,3,4			64.6°	3.1 Å	1.4 Å
	3,4,5			79.7°	2.8 Å	0.5 Å
	2,3,4,5,6[a]			79.1°	2.9 Å	0.6 Å

[a] X-ray structure reported by Kim and colleagues (ref 15). [b] Ring centroid to ring centroid to C-4 benzyl carbon angle (for 4-, and 2,4-SBB derivatives) or carbonyl oxygen to ring centroid to C-4 benzyl carbon angle (for 2,3,4-, 3,4,5-, and 2,3,4,5,6-SBB derivatives). [c] Ring centroid to ring centroid distance (for 4-, and 2,4- SBB derivatives) or carbonyl oxygen to ring centroid distance (for 2,3,4-, 3,4,5-, and 2,3,4,5,6-SBB derivatives). [d] Horizontal displacement between the two ring centroids (for 4-, and 2,4-SBB derivatives) or between carbonyl oxygen and ring centroid (for 2,3,4-, 3,4,5-, and 2,3,4,5,6-SBB derivatives).

Figure 5. Superposition of inhibitor−inhibitor interactions; protein atoms are omitted for clarity. In each stereopair, inhibitors occupying the primary and secondary binding sites are on the right and left, respectively (the active site zinc ion is in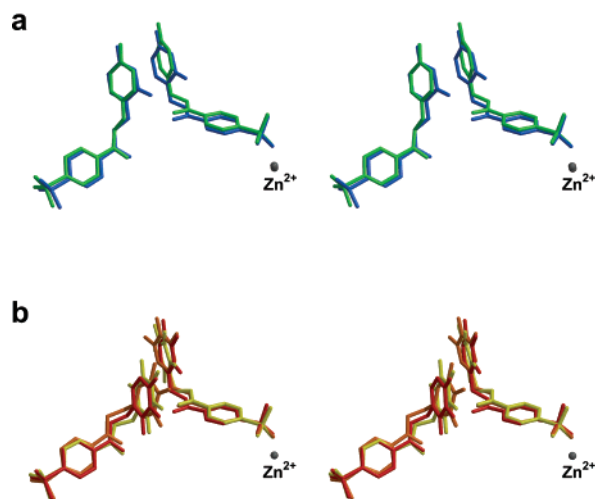 the primary binding site). (a) Face-to-face fluoroaromatic−fluoroaromatic interactions: 4-fluoro-SBB (green), 2,4-difluoro-SBB (blue). (b) Atom-to-face carbonyl−fluoroaromatic interactions: 2,3,4-trifluoro-SBB (red), 3,4,5-trifluoro-SBB (orange), 2,3,4,5,6-pentafluoro-SBB (yellow).

of the fluoroaromatic ring in the secondary binding site (Figure 5b). Because of the wide intermolecular cleft that accommodates the fluoroaromatic rings, face-to-face geometry is not sterically prohibited. For these three inhibitors, what energetic contributions dominate the altered binding conformation of the second fluoroaromatic ring relative to the less-fluorinated analogues discussed in the previous paragraph? For each of the three inhibitors, the carbonyl group of the inhibitor in the primary binding site is perpendicular to the face of the fluoroaromatic ring of the inhibitor in the secondary binding site. Because the interacting surface area in such an atom-to-face complex is very

small, van der Waals interactions likely contribute little. Therefore, dipole−quadrupole electrostatic interactions (Figure 6e) and charge-transfer complexation (Figure 6f) must dominate the observed fluoroaromatic−carbonyl interactions. First, consider the dipole−quadrupole electrostatic interaction: the positive quadrupole moment of the 2,3,4,5,6-pentafluorobenzyl group (Table 3) interacts favorably with the partial negative charge of the carbonyl oxygen atom. On the other hand, the 2,3,4- and 3,4,5-trifluorobenzyl groups have negative quadrupole moments (Table 3), so the interaction with the carbonyl oxygen is repulsive. Despite the attractive or repulsive contribution of dipole−quadrupole interactions, each inhibitor pair maintains a fluoroaromatic−carbonyl interaction. Therefore, it is possible that attractive sp^2→π* charge-transfer complexation governs the fluoroaromatic ring conformation. Thus, we again conclude that potential charge-transfer complexation dominates over weakly polar interactions (e.g., dipole−dipole, quadrupole−quadrupole) in the binding of these fluoroaromatic inhibitor pairs.

It is interesting that mono- or difluorinated aromatic ring pairs exhibit face-to-face geometry, whereas the more highly tri- or pentafluorinated aromatic ring pairs prefer the aromatic−carbonyl interaction. Because a combination of van der Waals interactions and charge-transfer complexation, or charge-transfer complexation alone, appears to dominate fluoroaromatic ring interactions, what directs aromatic−aromatic versus aromatic−carbonyl interaction for the fluoroaromatic ring in the secondary binding site? If van der Waals interactions contribute to the face-to-face interaction geometries exhibited by the fluoroaromatic rings of 4-fluoro-SBB and 2,4-difluoro-SBB, then face-to-face geometry ought to be even more favored for more highly fluorinated aromatic ring pairs. The atomic radii of fluorine and hydrogen are 1.40−1.47 Å and 1.06−1.20 Å, respectively,[23] and the C−F and C−H bond lengths are 1.399 and 1.059 Å, respectively.[24] Accordingly, the surface area of an aromatic ring

(21) Nicholls, A.; Sharp, K. A.; Honig, B. *Proteins: Struct., Funct., Genet.* **1991**, *11*, 281−296.
(22) Hernández-Trujillo, J.; Vela, A. *J. Phys. Chem. A* **1996**, *100*, 6524−6530.
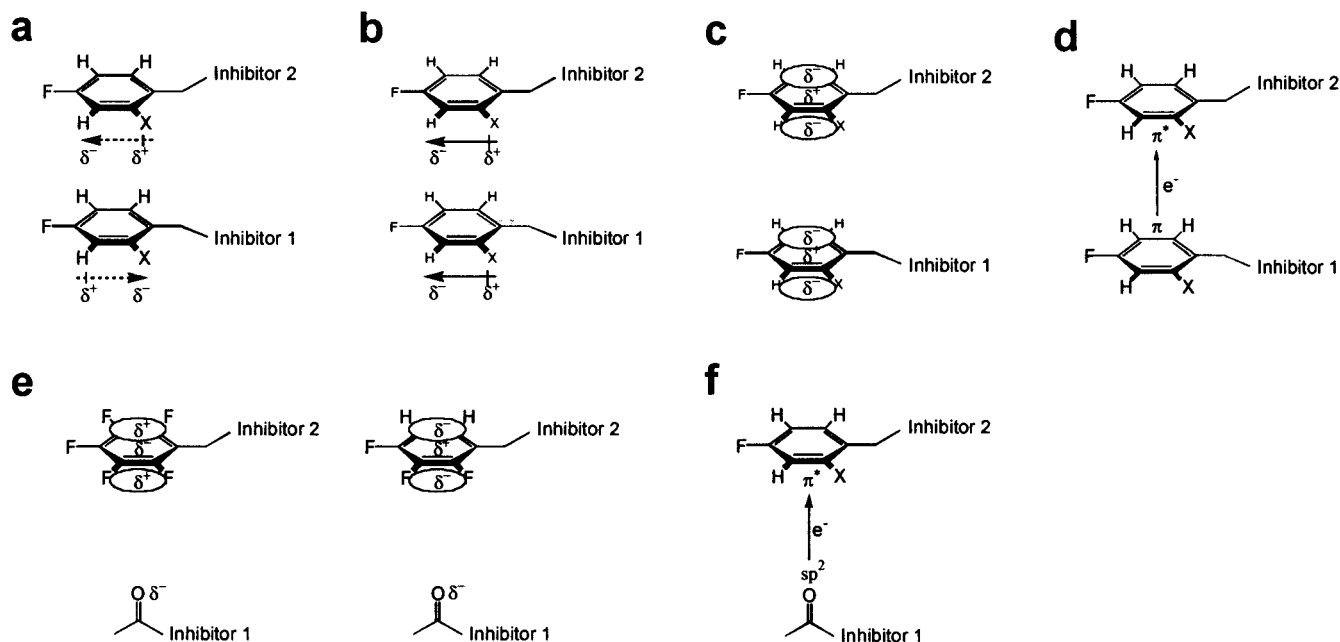(23) Bondi, A. *J. Phys. Chem.* **1964**, *68*, 441−451.

Figure 6. Intermolecular aromatic interactions discussed in the text. Face-to-face interaction: (a) induced-dipole−induced-dipole interaction (van der Waals interaction), (b) dipole−dipole electrostatic interaction, (c) quadrupole−quadrupole electrostatic interaction, (d) charge-transfer complexation. Atom-to-face interaction: (e) dipole−quadrupole electrostatic interaction, (f) charge-transfer complexation.

Table 3. Quadrupole Moments of Benzene and Fluorobenzenes

	Molecule	Surface area[a] (Å²)	Quadrupole moment[b], Q_{zz} (Buckingham)
	benzene	232	-8.56
	fluorobenzene	242	-6.33
	1,2-difluorobenzene	249	-4.60
	1,3-difluorobenzene	252	-3.17
	1,4-difluorobenzene	249	-2.31
	1,2,3-trifluorobenzene	258	-1.92
	1,3,5-trifluorobenzene	259	0.57
	pentafluorobenzene	274	6.11

[a] Solvent-accessible areas were calculated using GRASP[21] with a probe radius of 1.4 Å. [b] Ref 22. All molecules are centered on their centers of mass, and the z axis is perpendicular to the aromatic ring.

increases moderately with the degree of fluorine substitution (Table 3), and this could potentially enhance van der Waals interactions.

However, increased fluorination also diminishes the electron density in the π system of the aromatic ring, making it a weaker electron donor in a potential charge-transfer complex. The relatively electron-rich 4-fluorobenzyl and 2,4-difluorobenzyl groups are good electron donors, and the structures of their enzyme−inhibitor complexes reveal the π-stacking geometry required for potential charge-transfer complexation. On the other hand, the electron-poor 2,3,4-trifluoro-, 3,4,5-trifluoro-, and 2,3,4,5,6-pentafluorobenzyl groups are weak electron donors. With these more highly fluorinated inhibitors, then, the carbonyl oxygen of the first inhibitor is the better electron donor to the

fluoroaromatic ring of the second inhibitor. This simplified analysis again suggests that potential charge-transfer complexation dominates over weakly polar interactions (e.g., dipole−dipole, quadrupole−quadrupole) in the binding of these fluoroaromatic inhibitor pairs; moreover, potential charge-transfer complexation apparently dominates over van der Waals interactions in governing the conformation of more highly fluorinated inhibitor molecules occupying the secondary binding site.

Inhibitor Binding Stoichiometry. Unfortunately, there is no direct method for determining the dissociation constant, K_d, between the inhibitor and the secondary binding site in the crystal lattice. NMR experiments indicate a strict 1:1 binding ratio for all inhibitors in solution assays (data not shown), so the secondary binding site appears to be a unique consequence of crystal lattice formation. However, we can reasonably estimate the K_d for the secondary binding site by drawing inferences from the X-ray crystallographic results. We performed a titration study in which F131V CAII crystals were soaked for 7 days in solutions containing 1 mM, 100 μM, 50 μM, and 10 μM concentrations of 2,3,4,5,6-pentafluoro-SBB, and then we determined the X-ray crystal structure of each enzyme−inhibitor complex. At inhibitor concentrations of 50 μM or above, complete electron density for both inhibitors (one at each binding site) is observed; at 10 μM inhibitor concentration, weaker electron density is observed in the primary binding site and no density is seen in the secondary binding site (data not shown). We can estimate the K_d for the secondary binding site from the following relationship:

$$EI_2 \leftrightarrow EI + I \qquad K_d = \frac{[EI][I]}{[EI_2]}$$

where $[EI_2]$ is the concentration of enzyme with occupied secondary binding site, $[EI]$ is the concentration of enzyme with unoccupied secondary binding site, and $[I]$ is the concentration of free inhibitor. Because the inhibitor concentration (10 μM−1 mM) is much higher than the protein concentration in the crystal (approximately 0.1 μM), $K_d = [I]$ when $[EI] = [EI_2]$, that is,

(24) Lide, D. R. *CRC Handbook of Chemistry and Physics,* 80th Edition; CRC: Boca Raton, FL, 1999.

Table 4. Data Collection and Refinement Statistics for F131V CAII−inhibitor Complexes

	inhibitor					
	4-fluoro-SBB	2,4-difluoro-SBB	2,5-difluoro-SBB	2,3,4-trifluoro-SBB	2,4,6-trifluoro-SBB	3,4,5-trifluoro-SBB
no. measured reflections	94 989	125 993	124 216	112 884	108 937	128 567
no. unique reflections	19 121	22 021	21 474	21 403	19 532	23 524
max resolution (Å)	1.93	1.84	1.86	1.86	1.92	1.80
R_{merge}[a]	0.052	0.056	0.151	0.054	0.055	0.120
completeness of data (%)	95.8	90.6	96.3	91.5	92.9	95.1
no. reflections used in refinement ($>2\sigma$)	17 204	18 784	18 304	18 450	16 901	20 113
no. reflections in R_{free} test set	878	954	934	942	853	1022
R_{cryst}[b]	0.223	0.194	0.221	0.212	0.217	0.183
R_{free}[c]	0.280	0.256	0.280	0.278	0.290	0.240
no. nonhydrogen atoms[d]	2098	2100	2078	2102	2079	2102
no. solvent molecules	99	171	103	114	101	159
RMSD from ideal bond lengths (Å)	0.012	0.011	0.012	0.013	0.012	0.008
RMSD from ideal bond angles (Y)	1.6	1.6	1.7	1.6	1.7	1.5
RMSD from ideal dihedral angles (Y)	25.1	25.0	24.7	24.7	25.0	24.5
RMSD from ideal improper angles (Y)	1.4	1.4	1.5	1.4	1.4	1.3
RCSB accession code	1I9L	1I9M	1I9N	1I0O	1I9P	1I9Q

[a] R_{merge} for replicate reflections, $R = \Sigma |I_h - \langle I_h \rangle|/I_h$; I_h = intensity measured for reflection h; $\langle I_h \rangle$ = average intensity for reflection h calculated from replicate data. [b] Crystallographic R factor, $R_{cryst} = \Sigma||F_o| - |F_c||/\Sigma|F_o|$; $|F_o|$ and $|F_c|$ are the observed and calculated structure factor amplitudes, respectively, for those reflections not included in the R_{free} test set. [c] Free R factor, $R_{free} = \Sigma||F_o| - |F_c||/\Sigma|F_o|$ for only those reflections included in the R_{free} test set. [d] In asymmetric unit.

when half of the secondary binding sites in the crystal are occupied. Therefore, the K_d value for the secondary binding site is within the range $10-50$ μM. This represents approximately 10^4-fold weaker affinity compared with the nanomolar-affinity primary binding site (Table 1).

In the X-ray crystal structures of F131V CAII complexes with SBB, 2-fluoro-SBB, 2,3-difluoro-SBB, 2,5-difluoro-SBB, 2,6-difluoro-SBB, and 2,4,6-trifluoro-SBB, the secondary binding site is vacant; only the primary binding site is occupied, suggesting that for these inhibitors the secondary binding site K_d exceeds 50 μM. Given the wide cleft that accommodates inhibitor binding in the secondary site (Figure 2), it is puzzling that some inhibitors do not bind there under the conditions used to prepare crystalline enzyme−inhibitor complexes. Closer analysis of the structure of the complex with 2,4,6-trifluoro-SBB reveals that the fluoroaromatic group adopts a slightly different conformation compared with the other inhibitors, so as to block inhibitor association in the secondary binding site (Figure 4). Excluding this inhibitor because of its anomalous binding, then, we find that one common structural factor relates all of the inhibitors that occupy both primary and secondary binding sites: fluorine substitution at C-4. The C-2, C-3, and C-4 atoms of the fluoroaromatic ring in the secondary binding site make the closest contact with the inhibitor in the primary binding site (Figure 5): perhaps fluorination at C-4 is important for van der Waals contact and potential charge-transfer complexation between inhibitors. However, we cannot provide a completely satisfying explanation to correlate C-4 fluorination with inhibitor binding in the secondary site, and other phenomena involving the degree and pattern of fluorine substitution may also play a role.

Conclusions

Through the F131V amino acid substitution, the crystal lattice of CAII is engineered to accommodate two interacting fluoroaromatic inhibitors, thereby allowing us to systematically

evaluate the preferred structures of aromatic−aromatic interactions. Because the aromatic pair is not covalently linked, this system provides a true bimolecular aromatic−aromatic or aromatic−carbonyl association interaction that we can probe by varying the degree and pattern of fluorine substitution. For the aromatic−aromatic interactions investigated in this study, we conclude that the combined effects of London forces and charge-transfer complexation, or possibly charge-transfer complexation alone, dominate over weakly polar electrostatic interactions in the association of aromatic ring pairs.

Experimental Section

Crystals of recombinant F131V CAII were grown by the hanging drop method. Typically, 5 μL of protein solution ($8-12$ mg/mL protein, 1 mM methyl mercuric acetate, 50 mM Tris sulfate, pH 8.0) and 5 μL of precipitant buffer ($2.60-2.75$ M ammonium sulfate, 50 mM Tris sulfate, pH 8.0) were combined in a single drop hanging over a 1 mL reservoir of precipitant buffer at 4 °C. Crystals appeared within two weeks and were isomorphous with those of native CAII,[25] belonging to space group $P2_1$ with typical unit cell parameters $a = 42.7$ Å, $b = 41.4$ Å, $c = 72.9$ Å, and $\beta = 104.5°$.

Prior to the preparation of crystalline enzyme−inhibitor complexes, CAII crystals were cross-linked by adding 5 μL of glutaraldehyde solution (0.8% glutaraldehyde (v/v), 4.0 M $(NH_4)_2SO_4$, 50 mM Tris sulfate, pH 8.0) to the hanging drop and equilibrating it at 4 °C for 72 h. Each crystal was then transferred to a 10 μL drop containing a stabilization buffer of 3.5 M $(NH_4)_2SO_4$ and 50 mM Tris sulfate, pH 8.0. Finally, 1 μL of inhibitor solution (10 mM inhibitor in DMSO) was added to this drop and allowed to equilibrate at 4 °C for one week. Inhibitors were synthesized as described,[26] and crystals of enzyme−inhibitor complexes were mounted in 0.7 mm glass capillaries.

X-ray diffraction data were collected at room temperature using an R-AXIS IIc image plate detector (Molecular Structure Corporation), with a Rigaku RU-200HB rotating anode generator (operating at 50

(25) Håkansson, K.; Carlsson, M.; Svensson, L. A.; Liljas, A. *J. Mol. Biol.* **1992**, *227*, 1192−1204.
(26) Doyon, J. B.; Jain, A. *Org. Lett.* **1999**, *1*, 183−185.

kV and 100 mA) supplying Cu Kα radiation focused with Yale double mirrors. Raw diffraction data were processed using the HKL suite of programs.[27]

The 1.54 Å resolution structure of native human CAII[25] retrieved from the Research Collaboratory for Structural Bioinformatics (RCSB; accession code = 2CBA) was used as the starting coordinate set for the refinement of each enzyme−inhibitor complex structure. Each structure was refined by simulated annealing with energy minimization as implemented in X-PLOR.[28] Inhibitor atoms and active site solvent molecules were added into electron density maps generated with Fourier

(27) Otwinowski, Z.; Minor, W. *Methods Enzymol.* **1997**, *276*, 307−326.

(28) Brünger, A. T.; Kuriyan, J.; Karplus, M. *Science* **1987**, *235*, 458−460.

coefficients $(2|F_o| - |F_c|)$ and $(|F_o| - |F_c|)$ and phases calculated from the refined model when the R-factor dropped below 0.20. Refinement converged smoothly to final crystallographic R-factors within the range 0.165−0.198. Data refinement and collection statistics for F131V CAII-inhibitor complexes are recorded in Table 4. Coordinates of all enzyme−inhibitor complexes have been deposited in the RCSB with accession codes designated in Table 4.

JA011034P